Chemistry & Biology, Vol. 10, 551–561, June, 2003, ©2003 Elsevier Science Ltd. All rights reserved. DOI 10.1016/S1074-5521(03)00121-2

The Mg^{2+} Binding Sites of the 5S rRNA Loop E Motif as Investigated by Molecular Dynamics Simulations

Pascal Auffinger,* Lukasz Bielecki, and Eric Westhof
Institut de Biologie Moléculaire et Cellulaire du CNRS
Modélisations et Simulations des Acides Nucléiques, UPR 9002
15 rue René Descartes
67084 Strasbourg Cedex
France

Summary

Molecular dynamics simulations have been used to investigate the binding of Mg^{2+} ions to the deep groove of the eubacterial 5S rRNA loop E. The simulations suggest that long-lived and specific water-mediated interactions established between the hydrated ions and the RNA atoms lining up the binding sites contribute to the stabilization of this motif. The Mg^{2+} binding specificity is modulated by two factors: (i) a required electrostatic complementarity and (ii) a structural correspondence between the hydrated ion and its binding pocket that can be estimated by its degree of dehydration and the resulting number and lifetime of the intervening water-mediated contacts. Two distinct binding modes for pentahydrated Mg^{2+} ions that result in a significant freezing of the tumbling motions of the ions are described, and mechanistic details related to the stabilization of nucleic acids by divalent ions are provided.

Introduction

Magnesium ions are essential cofactors involved in the folding [1, 2], structural stability [3], and catalytic activity [4] of many RNA molecules. Numerous structural data have uncovered several of their binding sites [5–7], and it has been emphasized that these ions bind preferentially to electronegative sites in two principal ways, namely "site bound" and "diffusely bound" (for a review, see [3]). From the structural point of view, Mg^{2+} ions can interact with RNA, most frequently, in a completely hydrated (six bound waters) or, more rarely, partially dehydrated (five or four bound waters) state. Yet, little is known about the factors that modulate their binding specificity and their dynamical behavior. Such knowledge would considerably increase our understanding of their modes of binding and action. In order to provide some insight into these issues, we carried out over 50 ns of molecular dynamics (MD) simulations on the internal loop E (LE; see Table 1 and Figure 1) fragment of the eubacterial 5S rRNA [8, 9].

The LE is a pseudosymmetric motif characterized by a phylogenetically highly conserved stack of 7 non-Watson-Crick base pairs [10]. It is known to constitute a specific binding site for the ribosomal protein L25 in *E. coli* [11, 12] or its counterpart TL5 in *Thermus thermophilus* [13]. Remarkably, the LE structure is not affected by the presence of protein ligands both in the crystal phase and in solution since, as shown by X-ray [12–14] and NMR [11, 15] data, it is analogous in its complexed and uncomplexed state [11, 13, 16]. Conversely, the structure of this motif is known to be highly sensitive to the presence or absence of divalent ions [9, 15, 17–19]. Hence, it is not surprising to find, in a high-resolution crystal structure [14], five Mg^{2+} ions bound to the deep/major groove of LE (Figure 1). Ions 1 and 2 are hexahydrated and contact the RNA through water-mediated interactions at the level of G105-G106 (ion 1) and G75-G76 (ion 2). Ion 3 is pentahydrated and forms a direct contact with (G98)O6. Ions 4A and 4B have been described as being part of a binuclear metal cluster in which three water molecules bridge the two ions that form 4A...OR(A101) and 4B...OR(G100) direct contacts (note that OR corresponds to O1P in the standard PDB nomenclature and to O2P in the PDB files listed in Table 1).

From the methodological point of view, it has been demonstrated that MD simulations are successful tools for the identification of sequence-specific monovalent ion binding sites in nucleic acids [20–25]. Furthermore, MD simulations have been used to evaluate the structural effects of highly charged $Co(NH_3)_6^{3+}$ ions on DNA helices [26]. Yet, despite their major structural and biochemical implications, the dynamical behavior of hydrated Mg^{2+} ions associated with nucleic acids has been relatively rarely investigated [27–35] mainly because of methodological difficulties associated with very long residence times of water molecules bound to these divalent ions (2–10 μs), which are several orders of magnitude longer than the residence times of water molecules bound to monovalent ions [36]. As such, these techniques cannot be used for simulating the desolvation process of Mg^{2+} ions associated with the formation of inner sphere complexes. However, they can provide useful data related to the dynamical behavior of ions located at their most favorable binding sites as detected by crystallography.

Here, seven simulations starting from the LE structure with the inclusion of zero, four, and five Mg^{2+} ions will be described and the limitations associated with the use of MD techniques will be addressed.

Results

Stability of the Binuclear Metal Cluster

The first simulation, named ***5Mg*** (1.95 ns), was performed on a model containing five Mg^{2+} ions (Figure 1). During the run, the distance separating the 4A and 4B ions belonging to the bimetallic cluster quickly reached an average value of ≈6.5 Å, far from the initial 2.7 Å value (Figure 2A). In an attempt to stabilize their positions, a distance constraint of 3000 kcal.Å^{-1} was applied be-

*Correspondence: p.auffinger@ibmc.u-strasbg.fr

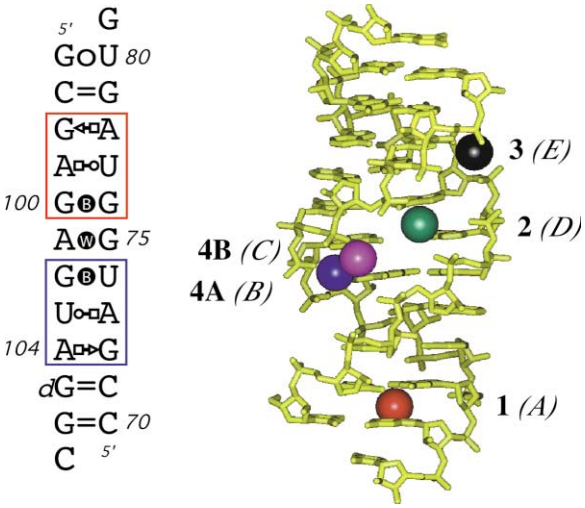

Figure 1. Loop E Fragment of the Bacterial 5S Ribosomal RNA

(Left) The two similar submotifs of the LE secondary structure are boxed. The symbols used for annotating the 2D structure are those proposed by Leontis and Westhof [65]: the two external A•G pairs are of the *trans* Hoogsteen sugar edge type, and the central G•A pair is of the water-mediated type; the U•A pairs are of the *trans* Watson-Crick/Hoogsteen type; the central G•U and G•G pairs are of the bifurcated type; and the terminal G•U pair is of the wobble type. Residue 105 is a deoxyriboguanosine. (Right) Crystallographic structure showing the five deep groove Mg^{2+} ions [14] is shown. The present Mg^{2+} numbering is shown in bold; the original labeling is placed in parenthesis.

tween them throughout simulation ***5Mg_Const*** (3.45 ns). This led to strong backbone distortions associated with a reorientation of the bimetallic cluster (Figure 2B).

Hence, models that integrate the information provided by the X-ray structure, namely two Mg^{2+} ions bridged by three water molecules, fail to reproduce the experimental intermetal distance. Thus, in line with other studies suggesting that bridging water molecules alone cannot stabilize two divalent ions separated by less than 3.0 Å [37, 38], the chemical identity of the bridging solvent molecules was questioned and other models compatible with the X-ray data were tested. First, as proposed earlier [30], one of the bridging water molecules was replaced by an OH^- ion (***5Mg_1OH***; 1.95 ns). Yet, during the equilibration phase, the hydroxide ion intercalated between the two Mg^{2+} ions increasing the intermetal distance from 2.7 to 4.5 Å (Figure 2C). In a second model (***5Mg_2OH***; 11.45 ns) that included two OH^- ions [37, 38], the intermetal distance stabilized around 3.0 Å (Figure 2D). However, a finer check involving the calculation of pseudoelectron densities (see Computational Methods section) revealed a blurred pattern associated with the two divalent ions (Figure 2E) pointing to certain shortcomings of this simulation.

Finally, a model in which the experimental diffraction patterns are interpreted in terms of alternative occupancies of the 4A and 4B binding sites, was tested. For that purpose, two simulations (***4MgA*** and ***4MgB***) each including one ion from the cluster (either 4A or 4B) were produced. The calculated pseudoelectron densities, obtained by combining the trajectories to a 1:1 ratio, reproduced quite well the X-ray positions of the two Mg^{2+} ions (Figure 2F) with deviations between the experimental and calculated positions for these atoms below 0.5 Å. Thus, this latter model, which is the most successful in reproducing the positions of the 4A and 4B ions, will be along with a control simulation that excludes Mg^{2+} ions (***NoMg***), the focus of subsequent analysis.

Structural Stability of the Loop E Motif

Before describing the ion-RNA interactions, the structural integrity of the LE motif has to be assessed. During the ***4MgA/B*** and ***NoMg*** trajectories, the rms deviations from the starting structure stabilized around 1.2–1.8 Å (Supplemental Figure S1; see Supplemental Data section) in accord with the 1.3 Å rms deviation calculated between the NMR and X-ray structures [15]. Given such reasonable values, the last 10 ns of trajectories ***4MgA***, ***4MgB***, and ***NoMg*** were analyzed in order to evaluate the stabilizing effects associated with Mg^{2+} ions.

In the absence of divalent ions, the LE motif displays a larger flexibility, as indicated by the per-residue *B factor* values calculated for all three trajectories (Supplemental Figure S2; see Supplemental Data section) and by the dynamics of the ribose groups, the backbone atoms, the stacking patterns, and the non-Watson-Crick pairs. In all trajectories, the prevalent conformation of the ribose rings was *C3′-endo*. Transient flips toward the *C2′-endo* pucker for nonterminal sugars occurred only in the ***NoMg*** simulation (for terminal sugars, short flips were observed in all simulations). The number of dihedral backbone transitions, observed essentially at GpA steps where an unusual cross-strand purine stack occurs [14], was the highest in the ***NoMg*** simulation in which additional transient unstacking events, absent from the ***4MgA/B*** simulations, were also observed [39].

In the ***4MgA/B*** simulations, all non-Watson-Crick pairs remain close to their experimental conformations. Yet, in the absence of Mg^{2+} ions, some pairs display a diminished stability (Supplemental Table S1; see Supplemental Data section) related to reversible "base pair opening events" occurring mainly in the later part of the trajectories. Therefore, for all base pairs (except

Table 1. List of Structures Containing the 22-Nucleotide-Long Eubacterial Loop E Motif and Number of Mg^{2+} Ions that Are Bound to the Deep Groove of This Fragment

Description	Abbreviation	Resolution (Å)	Mg^{2+} Ions	NDB/PDB Code	Reference
Eubacterial loop E motif	LE	1.5	5	url064/354d	[14]
Extended loop E motif	extended LE	3.0	5	url069/364d	[14]
Complex with L25	LE/L25	1.8	5	pr0018/1dfu	[12]
Complex with TL5	LE/TL5	2.3	3/4[a]	rr0012/1feu	[13]

[a] Two nonequivalent LE duplexes are present in the asymmetric unit of the LE/TL5 crystal.

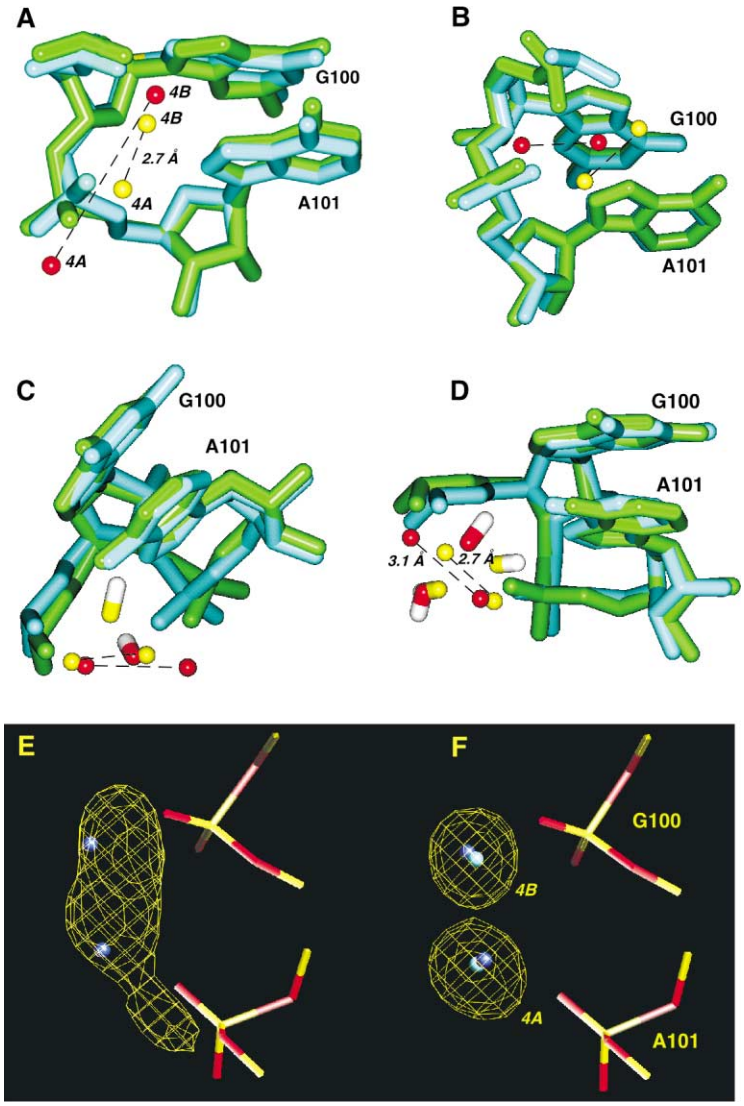

Figure 2. Stability of the Binuclear Mg^{2+} Cluster

(Top) Initial (yellow and cyan) and final (red and green) views extracted from the ***5Mg*** (A), ***5Mg_Const*** (B), ***5Mg_1OH*** (C), and ***5Mg_2OH*** (D) trajectories showing the ions 4A/B and the associated nucleotides G100-A101. In (C) and (D), the initial (yellow) and final (red) positions of the OH^- ions are shown (hydrogens are white). (Bottom) Pseudoelectron densities calculated over the last 10 ns of trajectory ***5Mg_2OH*** (E) and for a 1:1 combination of trajectories ***4MgA*** and ***4MgB*** (F). The initial positions of ions 4A and 4B are shown in blue (E and F), and the calculated average positions extracted from trajectories ***4MgA/B*** are shown in cyan (F).

A73•U103), the calculated average structures (over the last 10 ns) match their crystallographic counterpart. However, for the *trans* Watson-Crick/Hoogsteen A73•U103 pair in the ***NoMg*** simulation, a partial opening, characterized by a disruption of the (A)N7…H-N3(U) hydrogen bond, was observed (Supplemental Figure S3; see Supplemental Data section). Interestingly, the symmetrical U77•A99 pair that is embedded in a slightly different environment retained its configuration during all three trajectories.

Characterization of the Mg^{2+} Binding Sites

On the 10 ns time scale, although they display various dynamical behaviors, all ions remain close to their crystallographic position. Ions 4A and 4B, when they are considered in isolation of the bimetallic cluster to which they belong, retain their pentahydrated coordination (Figure 3 and Supplemental Figure S4; see Supplemental Data section) and occupy well-defined binding pockets (Figure 2F) characterized by stable 4A…OR(A101) and 4B…OR(G100) contacts (≈2.0 Å; Supplemental Table S1; see Supplemental Data section). The distances separating the X-ray and calculated positions of the 4A and 4B ions are below 0.5 Å (Supplemental Figure S3; see Supplemental Data section) and the rms deviations for the six atoms constituting the pentahydrated ions are close to 0.7 (4A) and 0.9 Å (4B). The major water-mediated contacts (Figure 4) are well maintained, although transient breakage of these interactions that can extend over a few tenths of a nanosecond are observed. In both simulations, a new mediated contact between ion 4A or 4B and (A73)OR, leading to a narrowing of the deep groove comparable to that observed in the extended LE structure, has been noted.

Ion 3 remains similarly pentahydrated (Figure 3 and Supplemental Figure S4; see Supplemental Data section) and the direct Mg^{2+}…O6(G98) as well as one water-mediated contact to (G76)OR are preserved (Figure 4). Besides, two temporarily broken water-mediated links to the (C97)OR and (G98)N7 atoms are detected. The distance separating the experimental and calculated position of ion 3 is close to 0.9 Å and the rms deviation

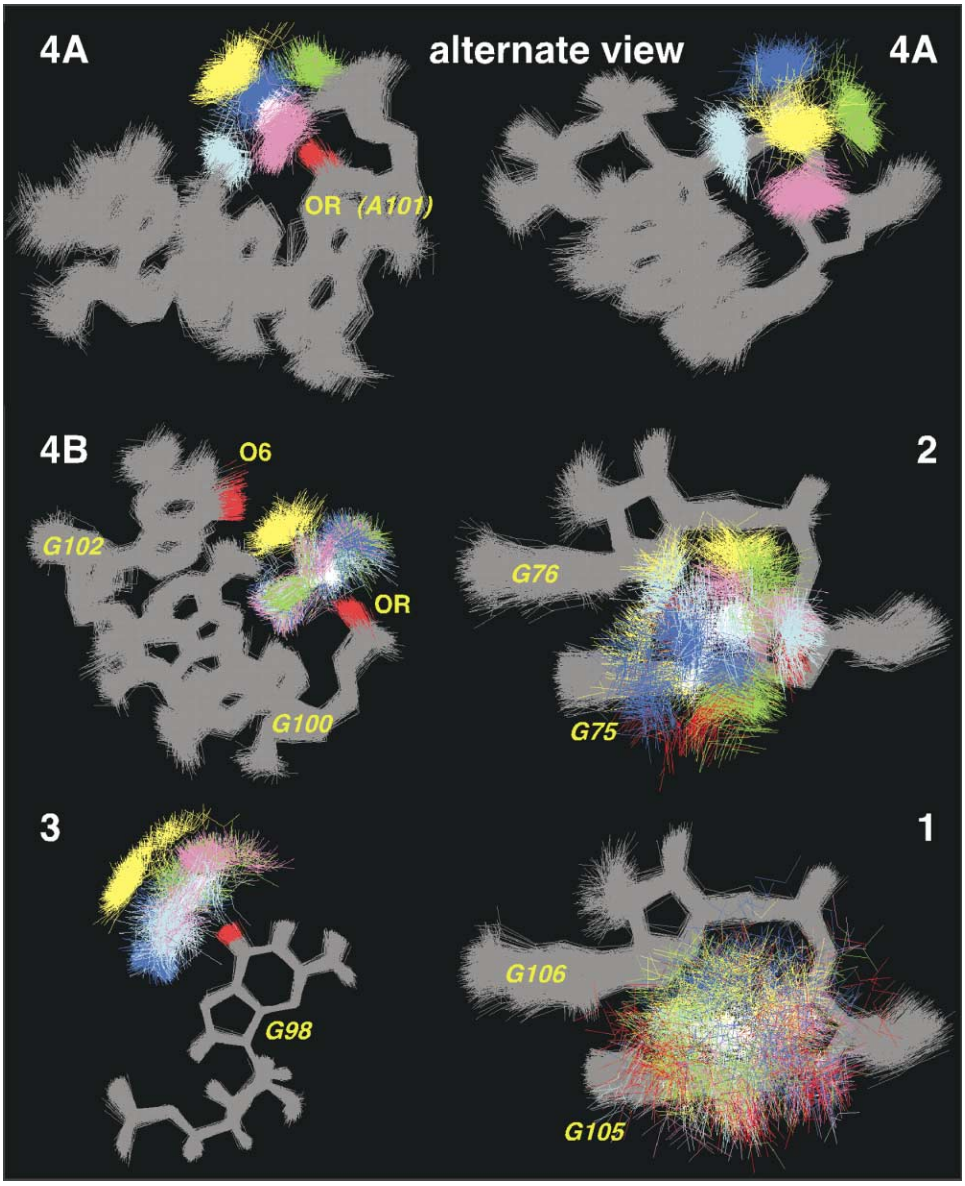

Figure 3. Superimposition of Snapshots Extracted from the ***4MgA/B*** Simulations Showing the First Hydration Shell of the Five Mg^{2+} Ions

According to Figure 4, a specific color is attributed to each water molecule (Mg^{2+} ions are white). For each of the pentahydrated ions 4A, 4B, and 3, the water molecule opposite to the direct Mg^{2+}…RNA contact (or apical water molecule) is yellow. The remaining four water molecules are of the equatorial type (see also Figures 4 and 6). For ion 4A, two views are provided: (top left) the Mg^{2+}...OR(A101) axis is included in the plane of the page; (top right) this axis is perpendicular to the plane of the page.

for the pentahydrated ion is close to 1.1 Å. Worth mentioning, the Mg^{2+}…O6(G98) distance shrinks from 2.6 to 2.1 Å soon after the beginning of both simulations (Supplemental Table S1; see Supplemental Data section) in better agreement with the customary 2.1 Å Mg^{2+}...O distance derived from high-resolution X-ray structures [40]. For the hexahydrated ions 1 and 2, most of the water-mediated contacts were maintained (Figure 4), and the distances separating the calculated and experimental positions of these ions are close to 0.8 (ion 1) and 1.4 Å (ion 2). Unfortunately, rms deviations for the hexahydrated ions could not be determined since the positions of only three (ion 1) and five (ion 2) water molecules instead of six were unambiguously assigned.

In conclusion: (i) the five ions retain a coordination shell similar to that observed in the crystal structure; (ii) the distances separating the calculated and experimental Mg^{2+} positions, that follows the order 4B (0.2 Å) $<$ 4A (0.5 Å) $<$ 1 (0.8 Å) $\approx$ 3 (0.9 Å) $<$ 2 (1.4 Å), are quite reasonable; (iii) the pentahydrated ions 4A and 4B are the closest to their crystallographic positions, while the hexahydrated ion 2 exhibits the largest deviations.

Dynamics of the Hydrated Mg^{2+} Ions

No exchange between the water molecules belonging to the first and second hydration shells of the Mg^{2+} ions has been observed during the simulations. Furthermore,

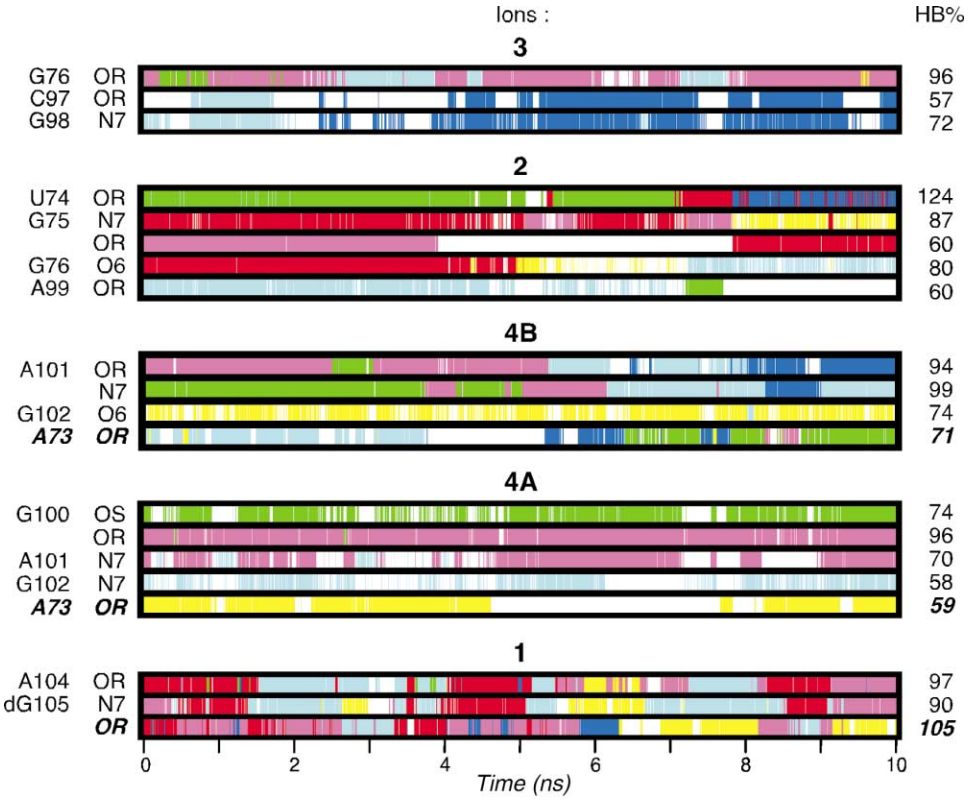

Figure 4. Dynamics of Water-Mediated Contacts

Dynamical characterization and hydrogen bond percentages (HB%) of water-mediated contacts formed between RNA atoms and Mg^{2+} ions calculated for the last 10 ns of the ***4MgA*** (ions 1, 2, 3, and 4A) and ***4MgB*** (ion 4B) trajectories (for a complete set of data, see Supplemental Figure S5 [see Supplemental Data section for URL]). Here, HB% are defined as the total number of hydrogen bonds formed between all the water molecules bound to a given ion and specific RNA atoms divided by the total number of configurations (only RNA atoms for which the HB% value exceeds 50% have been considered; new contacts formed during the trajectories are shown in bold). The contributions from both hydrogen atoms of a given water molecule have been summed up. If two water molecules bind to the same atom at the same time (see for example (U74)OR with HB% of 124), the one with the longest contact time is considered. The water molecule color code is identical to that used in Figure 3. Time frames where no hydrogen bonds involving first shell water molecules occur are shown in white. Given the resolution of the figure, interruptions shorter than 5 ps are hardly distinguishable.

the five or six first shell water molecules do not exchange with each other and form a rigid cage of solvent molecules surrounding the ion. Hence, the hydrated ions can be considered as rigid entities undergoing collective tumbling motions.

In contrast to first shell interactions, second sphere contacts display a large range of dynamical behaviors (Figures 3 and 4). For each of the hydrated ions, at least one of those contacts is characterized by hydrogen bonding percentage (HB%, see Figure 4) values higher than 90% revealing the occurrence of strong water-mediated interactions stabilizing the position of the ion with respect to its binding pocket. Yet, these interactions involve the participation of one or several water molecules depending on the type of reorientational motions associated with the ions. For instance, pentahydrated ion 4A is stabilized by a certain number of long-lived water-mediated contacts. The most persistent of them is formed between (G100)OR and an equatorial water molecule (HB% $\approx$ 96%). The binding of this single water molecule, which also forms transient bridges with (A101)N7, restricts significantly the motions of ion 4A. At the other extreme, the hexahydrated ion 1 reorients much more rapidly. Here, the tumbling motion of the ion allows all the coordinated water molecules to participate in almost each water-mediated contact during the 10 ns of the production run. The hexahydrated ion 2 shows an intermediate mobility characterized by longer-lived water-mediated contacts (Figure 4), and a rapid visual inspection suggests that the contacts established between this ion and its hydration site are more specific than those involving ion 1.

In order to get a better estimate of the complementarity existing between the hexahydrated ions and their binding pockets, the total number of hydrogen bonds formed during the simulations between first shell water molecules and RNA atoms has been calculated. These values, averaged over simulations ***4MgA*** and ***4MgB***, are 33% for ion 1 and 51% for ion 2 (note that a 100% value would imply that all 12 hydrogens of the 6 bound water molecules are involved in hydrogen bonds with RNA atoms). Thus, on the average, about four and six hydrogen atoms belonging to hexahydrated ions 1 and 2, respectively, are participating in hydrogen bonds with RNA atoms. The large disparity in the average number of hydrogen bond contacts established by these ions

is probably rooted in the different geometrical environment in which they are embedded: ions 1 and 2 bind to the deep groove of a Watson-Crick and a non-Watson-Crick GpG step, respectively.

Interestingly, for the pentahydrated ions 4A, 4B, and 3, the formation of a direct Mg^{2+}…RNA contact results in the immobilization of their apical water molecule (in yellow, Figure 4). As an outcome, the only allowed motions involve rotations of the equatorial water molecules around the Mg^{2+}…(OR or O6) axis with reorientation times that are related to the lifetime of their water-mediated interactions (Figures 3 and 4). Such in-plane motions of the equatorial water molecules are observed for ions 4B and 3 (the hydration shell of the latter appears the most mobile). Furthermore, contrary to ion 3 for which the apical water molecule displays a large mobility and is not involved in water-mediated interactions, the apical water molecule of ion 4B forms long-lived contacts with the (G102)O6 atom. This contact, although transiently broken (HB% ≈ 74%), is steady throughout the simulation. From these considerations, it results that ion 4B is stabilized by two contacts forming a clamp: (i) the direct Mg^{2+}…OR(G100) contact and (ii) the water-mediated contact involving (G102)O6. A similar clamp, that involves a contact with (A73)OR not observed in the crystal structure, stabilizes ion 4A.

The total number of hydrogen bonds formed during the simulations between the first shell water molecules of these pentahydrated ions and RNA atoms are of 44% for ion 4A, 36% for ion 4B, and 26% for ion 3. Thus, among the pentahydrated ions, ion 3 forms the smallest number of contacts and is probably occupying the weakest binding pocket while ions 4A and 4B establish a similar number of contacts. Hence, as for hexahydrated ions, the specificity of binding pockets toward pentahydrated ions similarly appears to correlate with the geometrical arrangement of their hydrophilic sites.

It is also worth noting that the binding of hydrated Mg^{2+} ions considerably increases the lifetime of second shell interactions. The maximum lifetimes of the hydrogen bonds involved in water-mediated interactions shown in Figure 4 range roughly from 0.4 to 2.5 ns (if a maximum interruption time of 2 ps for a given bond is considered). With more tolerant criteria, it can be seen that several water molecules are almost continuously bound to the same RNA atom over the 10 ns portion of the trajectories (see for example 4A… OR(G100)). Those values are significantly higher than the calculated ≈10 ps mean residence times of water molecules residing in the second hydration shell of unbound Mg^{2+} ions [41] and the maximum residence times of water molecules located in the deep groove of RNA duplexes (≈0.6 ns [21, 22]).

Hydration of the Bimetallic Cluster

As shown above, the model combining simulations ***4MgA*** and ***4MgB*** to a 1:1 ratio reproduces well the positions of the Mg^{2+} ions belonging to the bimetallic cluster. The superposition of the average structures indicates that the calculated 4A…4B distance of 2.5 Å is close to the original 2.7 Å distance (Figures 2F and 5) and that the 4A…OR(A101) and 4B…OR(G100) distances stabilize around 2.0 Å (Supplemental Table S1; see Supplemental Data section).

With this model, seven density peaks for water molecules were calculated around ions 4A and 4B. Three of them correspond to bridging water molecules while two others are completing the hydration sphere of each Mg^{2+} ion (Figure 5) by adopting positions similar to those observed in the crystal structure. The model was further improved by considering an occupancy ratio of 1:2 for the 4A and 4B ions leading to an rms value of 0.7 Å between the experimental and simulated positions of the atoms belonging to the cluster. Interestingly, in this last model, as in the crystal structure, one of the bridging water molecules is located at an unusual distance of ≈2.4 Å from each Mg^{2+} ion. Thus, considering the calculated data and the fact that we were unable to stabilize the Mg^{2+} cluster in the simulations (either by using constraints or bridging OH^- ions), it is reasonable to assume that fractional occupancies can be used to interpret the experimental electron densities.

Discussion

Mg^{2+} Ions Stabilize the Loop E Motif

In contrast to the ***NoMg*** simulation, no major disruption events of the seven non-Watson-Crick pairs could be detected in the ***4MgA/B*** simulations, and the overall dynamics of the base pairs is reduced (Supplemental Table S1; see Supplemental Data section). It can thus be concluded that magnesium contributes to the stabilization of the LE motif. This deduction is in line with several experimental studies showing that LE requires Mg^{2+} ions in order to maintain its 3D shape. For instance, chemical and enzymatic probing experiments demonstrate that LE is highly structured in the presence of Mg^{2+} ions [18], and NMR studies show that, in the absence of divalent cations, all imino resonances are altered revealing profound structural changes [15, 17]. Indeed, Mg^{2+}-induced stabilization is not observed to the same degree for all RNA duplexes. Based on optical melting experiments, it has been emphasized that the extent of stabilization achieved by magnesium for the eubacterial LE was three times larger than that observed for other duplexes including the related eukaryotic LE motif [19]. Yet, the number of divalent ions necessary to achieve in vivo stabilization is not precisely known and may range from one, as suggested by optical melting experiments [19], to five, as observed in the LE crystal structure on which present simulations are based. In the following, some clues will be given as to which hydrated ions interact the most specifically with their binding pocket and, consequently, as to which ions may contribute the most significantly to the in vivo stabilization of this RNA loop. Since present MD methodologies are not able to calculate the energetic contribution of each individual hydrated ion to the stabilization of the loop, our conclusions are based on their relative dynamics and mobility.

About Binuclear Metal Clusters in Nucleic Acids

Binuclear metal clusters are a key element of many important catalytic processes [42]. Yet, clusters with short M^{2+}…M^{2+} distances are rare [37]. For nucleic acids, a

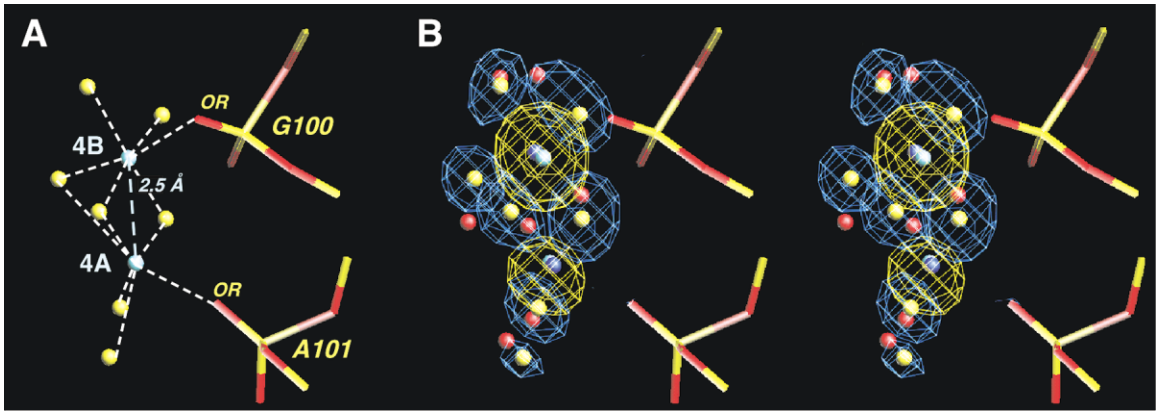

Figure 5. Experimental and Calculated Positions for the Ions and Water Molecules Belonging to the Mg^{2+} Cluster

(A) Calculated positions showing two Mg^{2+} ions and seven water molecules obtained by a superimposition (1:2 ratio) of the hydration shell of the 4A and 4B ions extracted from simulations ***4MgA*** and ***4MgB***. For this purpose, the hydration layers of the ions have been calculated up to 7.0 Å. Density not related to the water molecules of the first shell of both ions have subsequently been removed. The calculated 4A...4B distance is of 2.5 Å.

(B) Stereo view showing the calculated densities and the calculated and experimental positions of the atoms belonging to the Mg^{2+} cluster. In all panels, the calculated positions are shown in cyan (Mg^{2+}) and yellow (water); the X-ray positions are shown in blue (Mg^{2+}) and red (water).

survey of the nucleic acid database (NDB [43]) reveals five structures with intermetal distances below 3.0 Å, resolution better than 2.0 Å, and metal occupancies of 1.0 (url064, ddf027, zdf002, zdf052, zdf053). One of these clusters with an intermetal distance close to 2.8 Å is located in a 1.0 Å resolution structure of a Z-DNA hexamer (zdf002 [44]) and has been studied by MD simulations [28]. Similarly to what is observed in simulation ***5Mg***, the ions separated soon after the release of the initial constraints and, as in simulation ***5Mg_2OH***, the replacement of the two bridging water molecules by OH^- ions stabilized the intermetal distance close to 2.9 Å (see also [37]). In both cases, the Mg^{2+}…Mg^{2+} distance is close to 3.1 Å, exceeding by 0.4 the 2.7 Å distance reported for LE. Nevertheless, the arrangement of solvent molecules in LE (three bridging molecules) and in the complexes involving two OH^- ions (two bridging molecules) is significantly different.

A model with alternative and fractional occupancies of sites 4A and 4B is compatible with both the available diffraction data (C. Correll, personal communication) and with the alternative (or disordered) binding sites observed in crystal structures involving divalent [45–47] or divalent and monovalent ions [48, 49]. Hence, several hypotheses regarding the exact nature of the "bimetallic cluster" can be proposed. The most convincing model involves fractional occupancies of sites 4A and 4B. In such case, the LE structure would in fact contain no bimetallic cluster. Another possibility implies that an unknown arrangement of solvent molecules (water, OH^-, …) stabilizes the cluster. A model in which the complex begins to form only after site 4B is completely saturated cannot be excluded.

Finally, although an unambiguous view concerning the status of this cluster cannot be offered by the simulations, its characterization seems to be linked to specific crystallization conditions since site 4A is occupied only in the url064 structure (LE, see Table 1) and not in the other crystallized LE fragments (Supplemental Figure S6; see Supplemental Data section) while site 4B is occupied in all five X-ray structures. Furthermore, recent optical melting experiments put forward that only one strong Mg^{2+} binding site exists for LE in the liquid phase [19]. Overall, in solution and at physiological concentrations of Mg^{2+} ions, it is likely that only the site 4B is occupied. These conclusions support the approach consisting in investigating the binding of Mg^{2+} ions to the 4A and 4B sites in two independent trajectories.

Mechanistic Details Related to the Stabilization of RNA by Mg^{2+} Ions

Besides considerations relative to the bimetallic cluster, the present MD simulations allow a rough ranking of the Mg^{2+} binding sites with respect to the number and lifetime of water-mediated interactions involving the hydrated ions and the RNA atoms. For example, hexahydrated ions were found to interact more specifically with a non-Watson-Crick (site 2) than a canonical GpG step (site 1). This observation suggests that, with a comparable electrostatic contribution, the binding strength and specificity of an ion to a given site is modulated by the structural complementarity existing between the donor pattern of the hydrated ion (positions of the hydrogen atoms on the surface of the hydration sphere) and the acceptor pattern of the coordination pocket. Indeed, in the available LE crystal structures, site 1 is less often occupied by an Mg^{2+} ion than site 2 (Supplemental Figure S6; see Supplemental Data section).

For pentahydrated sites, the notion of structural complementarity is even more important and is associated with stereochemical constraints imposed by the formation of one direct Mg^{2+}…RNA contact. Such a contact results in the immobilization of the apical water molecule belonging to the coordination octahedron (see Figures 3 and 6) allowing only in-plane motions of the four equatorial water molecules. The tumbling motions of the hy-

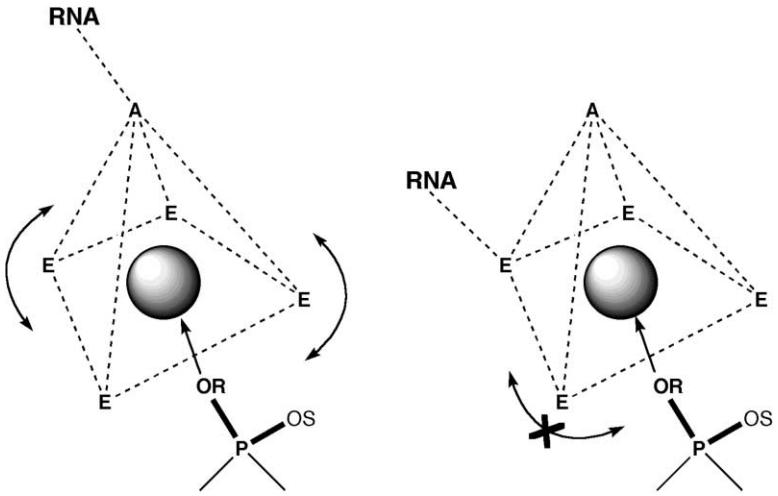

Figure 6. Two Types of Coordination Clamps Describing the Binding of Pentahydrated Mg^{2+} Ions

The ions are embedded into a rigid cage of solvent molecules and an OR atom completes the octahedral coordination of the ion. (Left: type *I*) When the immobilized apical water (A) molecule establishes a long-lived contact, the four equatorial water (E) molecules are still allowed to rotate; see ion 4B on Figure 3. (Right: type *II*) On the other hand, a long-lived water-mediated contact that involves one of the four equatorial water molecules completely immobilizes the first hydration shell; see ion 4A on Figure 3. Similar coordination clamps are possible for Mg^{2+} ions bound to OS, O2, O4, or O6 atoms.

dration shell can be further restrained by additional long-lived contacts involving the equatorial water molecules. The contacts that limit the motions of the hydrated ions, form the grips of coordination clamps. From the present observations, two major types of clamps could be characterized (Figure 6). In type *I*, long-lived water-mediated interactions involve the apical water molecule and do not hamper rotations of the equatorial water molecules (see ion 4B, Figure 3). In type *II*, an equatorial water molecule is fixed and freezes the entire hydration shell (see ion 4A, Figure 3). A combination of type *I* and *II* that implies the formation of very long-lived water-mediated contacts with the apical and, at least, one equatorial water molecule is also possible and would result in an optimal structural complementarity. Interestingly, related clamping motifs have been described for proteins [37].

Ion 3 is clearly not to be put into the preceding categories since it is the most mobile among the pentahydrated ions and forms very short water-mediated interactions with its equatorial water molecules. In fact, the occupation of this site is lattice dependent: in the two unbound LE structures, site 3 (close to G98) is occupied by an ion that establishes water-mediated contacts to the backbone of a symmetry-related molecule while the symmetric site 3′ (close to G72) is far from any RNA image and devoid of Mg^{2+} ions. Thus, such a site is not optimized for the stabilization of the LE motif, and the dynamics of the bound ion is restrained by the formation of intermolecular contacts rather than of strong contacts with its primary binding site.

Methodological Issues

Convergence of properties extracted from MD simulations is always difficult to assess [50, 51]. Based on MD simulations of DNA duplexes, it has been stated that reasonable equilibration times range from 5 to 25 ns [23]. Understandably, issues related to dehydration of $Mg(H_2O)_6^{2+}$ ions and formation of inner sphere complexes that take microseconds to occur [36] and may involve a deprotonation of a bound water molecule cannot be addressed by current MD techniques [31]. In spite of that, the behavior of the Mg^{2+} ions 1, 2, and 3 during the two independent ***4MgA*** and ***4MgB*** trajectories is comparable. Therefore, at least with respect to some properties, the simulations have converged on the 10 ns time scale. However, much longer simulations will be needed in order to provide a statistical evaluation of properties like the lifetimes of the water-mediated contacts shown on Figure 4.

Another important issue is associated with the point charge models that are used in MD simulations. These models do not explicitly consider important polarization and charge transfer effects [37, 52]. Unfortunately, inclusion of polarization and charge transfer effects is currently excessively difficult for systems of this size and over long time scales. Therefore, such simulations have not yet been attempted. Still, the calculated dynamics of the LE and its bound solvent molecules does not contradict available structural data pointing out that current empirical potentials provide a reasonable picture of the dynamical behavior of hydrated divalent species.

Significance

The present MD simulations, in agreement with numerous experimental data, support the view that Mg^{2+} ions contribute to the dynamical stabilization of the continuous stack of 7 non-Watson-Crick base pairs constituting the loop E (LE) motif by establishing long-lived direct and water-mediated contacts with the RNA atoms. The formation of such long-lived contacts is facilitated by the particular stereochemistry of the hydrated ions. Hexahydrated ions behave as rigid entities with 12 regularly spaced anchor points on their surface undergoing collective tumbling motions. Such ions are attracted to electronegative pockets with specificity in binding modulated by the structural complementarity which can be achieved by water-mediated contacts between them and the atoms lining up the fixation site.

On the other hand, pentahydrated ions, as a result of the direct Mg^{2+}…O interaction they form with RNA atoms, are able to establish strong water-mediated interactions through the formation of clamping motifs that involve the immobilized apical water molecule (opposite to the direct contact) and/or equatorial wa-

ter molecules. Two such clamping modes could be characterized. Generally, clamping motifs optimize the formation of long-lived second sphere interactions that, in turn, considerably reduce the tumbling motions of the hydrated ions and participate in the stabilization mechanism of nucleic acids by divalent ions. The understanding of the dynamics of water molecules located in the first hydration shell of Mg^{2+} ions and of the contacts they establish with RNA atoms is certainly of importance for deciphering the various structural and catalytic roles in which they are involved.

Computational Methods

Model Building

Seven simulations, based on a 1.5 Å resolution crystal structure [14], were performed (Supplemental Table S2; see Supplemental Data section). Simulation ***5Mg*** includes five Mg^{2+} ions (Figure 1). In simulation ***5Mg_Const***, a 3000 kcal.$Å^{-1}$ distance constraint was applied between ions 4A and 4B. In simulations ***5Mg_1OH*** and ***5Mg_2OH***, one or two water molecules bridging the 4A and 4B ions were replaced by OH^- ions. The two simulations ***4MgA*** and ***4MgB*** take into consideration a subset of four divalent ions which was obtained by splitting the bimetallic cluster, i.e., ***4MgA*** excludes 4B and ***4MgB*** excludes 4A. The simulation ***NoMg*** excludes all five Mg^{2+} ions.

The starting duplexes and Mg^{2+} ions were placed in a box containing SPC/E water molecules [53] in an amount necessary to ensure a 12 Å solvation shell around them (Supplemental Table S2; see Supplemental Data section). In order to neutralize these systems and achieve an ionic concentration close to 0.2 M of KCl, K^+ and Cl^- ions were added (even though Na^+ ions are present in the crystallization liquor [14], K^+ ions used in the NMR experiments [15] were considered). The ions were placed around the solute based on the electrostatic potential of the solvated system so that no ion was closer than 8 Å to any solute atom and 4 Å to any other ion.

MD Simulations

The simulations were run at constant temperature (298 K) and pressure (1 atm = 101,325 Pa) by using the AMBER 6.0 simulation package [54]. The calculations employed the all atom force field described by Cornell et al. [55]. The van der Waals parameters for the K^+ and Cl^- ions, calibrated for the SPC/E water model, were extracted from the following studies: [56, 57]. The Mg^{2+} parameters were extracted from the AMBER force field, and the OH^- parameters were extracted from the MD investigation: [28]. Given the instabilities associated with the positions of the ions belonging to the bimetallic cluster, simulations ***5Mg*** (1.95 ns), ***5Mg_Const*** (3.45 ns), and ***5Mg_1OH*** (1.95 ns) were interrupted at an early stage (Table S2; see Supplemental Data section). The simulations ***5Mg_2OH***, ***4MgA/B***, and ***NoMg*** were pursued up to 11.45 ns. The particle mesh Ewald (PME) summation method was used for the treatment of the long-range electrostatic interactions [58]. The charge grid spacing was chosen to be close to 1 Å and a cubic interpolation scheme was used. The trajectories were run with a time step of 2 fs by using SHAKE bond constraints. The equilibration procedure is similar to those reported elsewhere [21, 22]. First, the system was minimized by using 500 steps of steepest descent without positional constraints. This was followed by two 25 ps runs of MD (at 298 K), the first with only moving water molecules, the second with moving water molecules and K^+Cl^- ions. Then, eight 50 ps runs of MD were performed with positional constraints on the nucleic acid and Mg^{2+} ions of 10, 5, 2, 1, 0.5, 0.1, 0.01, and 0.001 kcal.$mol^{-1}Å^2$, respectively, yielding the equilibration phase which also comprised the first nanosecond of the subsequent nonconstrained MD run for a total of 1.45 ns (Figure S1; see Supplemental Data section). The saved trajectories were subjected to conformational analysis using the AMBER package tools and our own procedures.

The ion and water pseudoelectron densities were calculated using a procedure originally developed by Schneider and Berman [59] and adapted by us [21, 22, 60, 61]. Solvent molecules were placed in the calculated densities using the PEAKMAX program of the CCP4 library (http://www.dl.ac.uk/CCP/CCP4 [62]). The O8 program was used to visualize the "pseudoelectron" densities [63] and the MDdraw program to visualize the trajectories [64]. The following criteria: d(H…A) < 2.5 Å and θ(D − H…A) $> 135°$, where A stands for a hydrogen bond acceptor and D for a hydrogen bond donor atom, were used for calculating hydrogen bonds.

Supplemental Data

Supplemental Data includes Figures S1–S6 and Tables S1 and S2 and can be found at http://www.chembiol.com/cgi/content/full/10/6/551/DC1 and http://www-ibmc.u-strasbg.fr/upr9002/westhof/.

Acknowledgments

The authors wish to thank C. Correll for providing data and helpful discussions. L.B. acknowledges the E.C. Marie Curie fellowship. Computer time was provided in part by the Poznan Supercomputer and Networking Center and the ICPS (Images et Calcul Parallèle Scientifique) Strasbourg.

Received: March 14, 2003
Revised: April 23, 2003
Accepted: April 30, 2003
Published: June 20, 2003

References

1. Misra, V.K., and Draper, D.E. (2002). The linkage between magnesium binding and RNA folding. J. Mol. Biol. *317*, 507–521.
2. Serebrov, V., Clarke, R.J., Gross, H.J., and Kisselev, L. (2001). Mg^{2+}-induced tRNA folding. Biochemistry *40*, 6688–6698.
3. Misra, V.K., and Draper, D.E. (1998). On the role of magnesium ions in RNA stability. Biopolymers *48*, 113–135.
4. Fedor, M.J. (2002). The role of metal ions in RNA catalysis. Curr. Opin. Struct. Biol. *12*, 289–295.
5. Juneau, K., Podell, E., Harrington, D.J., and Cech, T.R. (2001). Structural basis of the enhanced stability of a mutant ribozyme domain and a detailed view of RNA-solvent interactions. Structure *9*, 221–231.
6. Jovine, L., Djordjevic, S., and Rhodes, D. (2000). The crystal structure of yeast phenylalanine tRNA at 2.0 Å resolution: cleavage by Mg(2+) in 15-year old crystals. J. Mol. Biol. *301*, 401–414.
7. Egli, M. (2002). DNA-cation interactions: quo vadis? Chem. Biol. *9*, 277–286.
8. Barciszewska, M.Z., Szymanski, M., Erdmann, V.A., and Barciszewski, J. (2001). Structure and functions of 5S rRNA. Acta Biochim. Pol. *48*, 191–198.
9. Moore, P.B. (1996). The structure and function of 5S ribosomal RNA. In Ribosomal RNA: Structure, Evolution, Processing, and Function in Protein Biosynthesis, R.A. Zimmermann and A.E. Dahlberg, eds. (London: CRC Press), pp. 199–236.
10. Leontis, N.B., and Westhof, E. (1998). The 5S rRNA loop E: chemical probing and phylogenetic data versus crystal structure. RNA *4*, 1134–1153.
11. Stoldt, M., Wöhnert, J., Ohlenschläger, O., Görlach, M., and Brown, L.R. (1999). The NMR structure of the 5S rRNA E-domain-protein L25 complex shows preformed and induced recognition. EMBO J. *18*, 6508–6521.
12. Lu, M., and Steitz, T.A. (2000). Structure of *Escherichia coli* ribosomal protein L25 complexed with a 5S rRNA fragment at 1.8-Å resolution. Proc. Natl. Acad. Sci. USA *97*, 2023–2028.
13. Fedorov, R., Meshcheryakov, V., Gongadze, G., Fomenkova, N., Nevskaya, N., Selmer, M., Laurberg, M., Kristensen, O., Al-Karadaghi, S., Liljas, A., et al. (2001). Structure of ribosomal protein TL5 complexed with RNA provides new insights into the CTC family of stress proteins. Acta Crystallogr. D *57*, 968–976.
14. Correll, C.C., Freeborn, B., Moore, P.B., and Steitz, T.A. (1997). Metals, motifs and recognition in the crystal structure of a 5S rRNA domain. Cell *91*, 705–712.
15. Dallas, A., and Moore, P.B. (1997). The loop E-loop D region of *Escherichia coli* 5S rRNA: the solution structure reveals an unusual loop that may be important for binding ribosomal proteins. Structure *5*, 1639–1653.

16. Rife, J.P., Stallings, S.C., Correll, C.C., Dallas, A., Steitz, T.A., and Moore, P.B. (1999). Comparison of the crystal and solution structures of two RNA oligonucleotides. Biophys. J. *76*, 65–75.
17. Leontis, N.B., Ghosh, P., and Moore, P.B. (1986). Effect of magnesium ion on the structure of the 5S RNA from *Escherichia coli*. An imino proton magnetic resonance study of the helix I, IV, and V regions of the molecule. Biochemistry *25*, 7386–7392.
18. Romby, P., Westhof, E., Toukifimpa, R., Mache, R., Ebel, J.P., Ehresmann, C., and Ehresmann, B. (1988). Higher order structure of chloroplastic 5S ribosomal RNA from spinach. Biochemistry *27*, 4721–4730.
19. Serra, M.J., Baird, J.D., Dale, T., Fey, B.L., Retatagos, K., and Westhof, E. (2002). Effects of magnesium ions on the stabilization of RNA oligomers of defined structures. RNA *8*, 307–323.
20. Young, M.A., Jayaram, B., and Beveridge, D.L. (1997). Intrusion of counterions into the spine of hydration in the minor groove of B-DNA: fractional occupancy of electronegative pockets. J. Am. Chem. Soc. *119*, 59–69.
21. Auffinger, P., and Westhof, E. (2000). Water and ion binding around RNA and DNA (C,G)-oligomers. J. Mol. Biol. *300*, 1113–1131.
22. Auffinger, P., and Westhof, E. (2001). Water and ion binding around $r(UpA)_{12}$ and $d(TpA)_{12}$ oligomers—comparison with RNA and DNA $(CpG)_{12}$ duplexes. J. Mol. Biol. *305*, 1057–1072.
23. Cheatham, T.E., 3rd, and Young, M.A. (2000). Molecular dynamics simulation of nucleic acids: successes, limitations, and promise. Biopolymers *56*, 232–256.
24. Feig, M., and Pettitt, B.M. (1999). Sodium and chlorine ions as part of the DNA solvation shell. Biophys. J. *77*, 1769–1781.
25. Korolev, N., Lyubartsev, A.P., Laaksonen, A., and Nordenskiold, L. (2002). On the competition between water, sodium ions, and spermine ion binding to DNA: a molecular dynamics computer simulation study. Biophys. J. *82*, 2860–2875.
26. Cheatham, T.E., and Kollman, P.A. (1997). Insight into the stabilization of A-DNA by specific ion association: spontaneous B-DNA to A-DNA transitions observed in molecular dynamics simulations of $d(ACCCGCGGGT)_2$ in the presence of hexaamminecobalt(III). Structure *15*, 1297–1311.
27. Young, M.A., and Beveridge, D.L. (1998). Molecular dynamics simulations of an oligonucleotide duplex with adenine tracts phased by a full helix turn. J. Mol. Biol. *281*, 675–687.
28. Lee, H., Darden, T.A., and Pedersen, L.G. (1995). Molecular dynamics simulation studies of a high resolution Z-DNA crystal. J. Chem. Phys. *102*, 3830–3834.
29. Hermann, T., Auffinger, P., Scott, W.G., and Westhof, E. (1997). Evidence for a hydroxide ion bridging two magnesium ions at the active site of the hammerhead ribozyme. Nucleic Acids Res. *25*, 3421–3427.
30. Hermann, T., Auffinger, P., and Westhof, E. (1998). Molecular dynamics investigations of the hammerhead ribozyme RNA. Eur. Biophys. J. *27*, 153–165.
31. Bevan, D.R., Li, L., Pedersen, L.G., and Darden, T.A. (2000). Molecular dynamics simulations of the $d(CCAACGTTGG)_2$ decamer: influence of the crystal environment. Biophys. J. *78*, 668–682.
32. Sprous, D., Young, M.A., and Beveridge, D.L. (1999). Molecular dynamics studies of axis bending in $d(G_5\text{-}(GA_4T_4C)_2\text{-}C_5)$ and $d(G_5\text{-}(GT_4A_4C)_2\text{-}C_5)$: effects of sequence polarity on DNA curvature. J. Mol. Biol. *285*, 1623–1632.
33. MacKerell, A.D. (1997). Influence of magnesium ions on duplex DNA structural, dynamic, and solvation properties. J. Phys. Chem. B *101*, 646–650.
34. Torres, R.A., and Bruice, T.C. (1998). Molecular dynamics study displays near in-line attack conformations in the hammerhead ribozyme self-cleavage reaction. Proc. Natl. Acad. Sci. USA *95*, 11077–11082.
35. Torres, R.A., and Bruice, T.C. (2000). The mechanism of phosphodiester hydrolysis—near in-line attack conformations in the hammerhead ribozyme. J. Am. Chem. Soc. *122*, 781–791.
36. Ohtaki, H. (2001). Ionic solvation in aqueous and nonaqueous solutions. Monatshefte für Chemie *132*, 1237–1268.
37. Glusker, J.P., Katz, A.K., and Bock, C.W. (2001). Two-metal binding motifs in protein crystal structures. Struct. Chem. *12*, 323–341.
38. Lee, H., Darden, T., and Pedersen, L. (1995). Accurate crystal molecular dynamics simulations using particle-mesh-Ewald: RNA dinucleotides—ApU and GpC. Chem. Phys. Lett. *243*, 229–235.
39. Bielecki, L., and Adamiak, R.W. (2001). Structure and dynamics of a DNA duplex containing single alpha-anomeric deoxyadenosine residue. Acta Biochim. Pol. *48*, 103–111.
40. Markham, G.D., Glusker, J.P., and Bock, C.W. (2002). The arrangement of first and second-sphere water molecules in divalent magnesium complexes: results from molecular orbital and density functional theory and from structural crystallography. J. Phys. Chem. B *106*, 5118–5134.
41. Martinez, J.M., Pappalardo, R.R., and Marcos, E.S. (1999). First-principles ion-water interaction potentials for highly charge monoatomic cations. Computer simulations of Al^{3+}, Mg^{2+}, and Be^{2+} in water. J. Am. Chem. Soc. *121*, 3175–3184.
42. Wilcox, D.E. (1996). Binuclear metallohydrolases. Chem. Rev. *96*, 2435–2458.
43. Berman, H.M., Olson, W.K., Beveridge, D.L., Westbrook, J., Gelbin, A., Demeny, T., Hsieh, S.H., and Srinivasan, A.R. (1992). The nucleic acid database: a comprehensive relational database of three-dimensional structures of nucleic acids. Biophys. J. *63*, 751–759.
44. Gessner, R.V., Frederick, C.A., Quigley, G.J., Rich, A., and Wang, A.H.J. (1989). The molecular structure of the left-handed Z-DNA double helix at 1.0 Å atomic resolution. Geometry, conformation, and ionic interactions of d(CGCGCG). J. Biol. Chem. *264*, 7912–7935.
45. Xiong, Y., Deng, J., Sudarsanakumar, C., and Sundaralingam, M. (2001). Crystal structure of an RNA duplex $r(GUGUCGCAC)_2$ with uridine bulges. J. Mol. Biol. *313*, 573–582.
46. Chiu, T.K., and Dickerson, R.E. (2000). 1 Å crystal structures of B-DNA reveal sequence-specific binding and groove-specific bending of DNA by magnesium and calcium. J. Mol. Biol. *301*, 915–945.
47. Robinson, H., Gao, Y.G., Sanishvili, R., Joachimiak, A., and Wang, A.H. (2000). Hexahydrated magnesium ions bind in the deep major groove and at the outer mouth of A-form nucleic acid duplexes. Nucleic Acids Res. *28*, 1760–1766.
48. Howerton, S.B., Sines, C.C., VanDerveer, D., and Williams, L.D. (2001). Locating monovalent cations in the grooves of B-DNA. Biochemistry *40*, 10023–10031.
49. Batey, R.T., Rambo, R.P., Lucast, L., Rha, B., and Doudna, J.A. (2000). Crystal structure of the ribonucleoprotein core of the signal recognition particle. Science *287*, 1232–1239.
50. van Gunsteren, W.F., and Mark, A.E. (1998). Validation of molecular dynamics simulations. J. Chem. Phys. *108*, 6109–6116.
51. Caspar, D.L.D. (1995). Problems in simulating macromolecular movements. Structure *3*, 327–329.
52. Munoz, J., Sponer, J., Hozba, P., Orozco, M., and Luque, F.J. (2001). Interactions of hydrated Mg^{2+} cation with bases, base pair, and nucleotides. Electron topology, natural bond orbital, electrostatic, and vibrational study. J. Chem. Phys. B *105*, 6051–6060.
53. Berendsen, H.J.C., Grigera, J.R., and Straatsma, T.P. (1987). The missing term in effective pair potential. J. Phys. Chem. *97*, 6269–6271.
54. Case, D.A., Pearlman, D.A., Caldwell, J.W., Cheatham, T.E., Ross, W.S., Simmerling, C.L., Darden, T.A., Merz, K.M., Stanton, R.V., Cheng, A.L., et al. (1999). AMBER 6, University of California, San Francisco.
55. Cornell, W.D., Cieplak, P., Bayly, C.I., Gould, I.R., Merz, K.M., Ferguson, D.M., Spellmeyer, D.C., Fox, T., Caldwel, J.W., and Kollman, P.A. (1995). A second generation force field for the simulation of proteins, nucleic acids, and organic molecules. J. Am. Chem. Soc. *117*, 5179–5197.
56. Dang, L.X. (1995). Mechanism and thermodynamics of ion selectivity in aqueous solutions of 18-crown-6 ether: a molecular dynamics study. J. Am. Chem. Soc. *117*, 6954–6960.
57. Dang, L.X., and Kollman, P.A. (1990). Free energy of association of the 18-crown-6:K^+ complex in water: a molecular dynamics simulation. J. Am. Chem. Soc. *112*, 5716–5720.
58. Darden, T., Perera, L., Li, P., and Pedersen, L. (1999). New tricks for modelers from the crystallography toolkit: the particle mesh

Ewald algorithm and its use in nucleic acid simulations. Structure *7*, R55–R60.
59. Schneider, B., and Berman, H.M. (1995). Hydration of the DNA bases is local. Biophys. J. *69*, 2661–2669.
60. Auffinger, P., and Westhof, E. (1998). RNA base pair hydration. J. Biomol. Struct. Dyn. *16*, 693–707.
61. Auffinger, P., Masquida, B., and Westhof, E. (2002). Structural and dynamical characterization of the nucleic acid water and ion binding sites. In Computational Methods for Macromolecules: Challenges and Applications, Volume 24, T. Slick and H.H. Gan, eds. (Heidelberg: Springer Verlag), pp. 61–70.
62. CCP4 (Collaborative Computational Project 4 (1994). The CCP4 suite: programs for protein crystallography. Acta Cryst. D *50*, 760–763.
63. Jones, T.A., Zou, J.Y., Cowan, S.W., and Kejldgaard, M. (1991). Improved methods for building protein models in electron density maps and the location of errors in these models. Acta Crystallogr. A *47*, 110–119.
64. Engler, E., and Wipff, G. (1994). MD Draw: a Program of Graphical Representation of Molecular Dynamics Trajectories (Strasbourg, FR: Université Louis Pasteur de Strasbourg).
65. Leontis, N.B., and Westhof, E. (1998). Conserved geometrical base pairing patterns in RNA. Q. Rev. Biophys. *31*, 399–455.